Publ. Astron. Soc. Japan (2020) 72 (2), 29 (1–11)
doi: 10.1093/pasj/psaa004
Advance Access Publication Date: 2020 March 2

ALMA band 8 observations of DLA 2233+131 at $z = 3.150$

Kazuyuki Ogura,[1,*] Hideki Umehata,[2] Yoshiaki Taniguchi,[3] Yuichi Matsuda,[4] Nobunari Kashikawa,[5] Kartik Sheth,[6] Katsuhiro Murata,[7] Masaru Kajisawa,[8,9] Masakazu A. R. Kobayashi,[10] Takashi Murayama,[11] and Tohru Nagao[9]

[1]Faculty of Education, Bunkyo University, 3337 Minamiogishima, Koshigaya, Saitama 343-8511, Japan
[2]RIKEN Cluster for Pioneering Research, 2-1 Hirosawa, Wako, Saitama 351-0198, Japan
[3]The Open University of Japan, 2-11 Wakaba, Mihama-ku, Chiba, Chiba 261-8586, Japan
[4]National Astronomical Observatory of Japan, 2-21-1 Osawa, Mitaka, Tokyo 181-8588, Japan
[5]Department of Astronomy, Graduate School of Science, The University of Tokyo, 7-3-1 Hongo, Bunkyo, Tokyo 113-0033, Japan
[6]NASA Headquarters, Washington, DC 20546-0001, USA
[7]Department of Physics, Tokyo Institute of Technology, 2-12-1 Ookayama, Meguro, Tokyo 152-8551, Japan
[8]Graduate School of Science and Engineering, Ehime University, Bunkyo-cho, Matsuyama, Ehime 790-8577, Japan
[9]Research Center for Space and Cosmic Evolution, Ehime University, 2-5 Bunkyo-cho, Matsuyama, Ehime 790-8577, Japan
[10]Faculty of Natural Sciences, National Institute of Technology, Kure College, 2-2-11, Agaminami, Kure, Hiroshima 737-8506, Japan
[11]Astronomical Institute, Graduate School of Science, Tohoku University, Aramaki, Aoba, Sendai, Miyagi 980-8578, Japan

*E-mail: ogurakz@koshigaya.bunkyo.ac.jp

Received 2019 August 6; Accepted 2020 January 15

Abstract

We present our ALMA Band 8 observations of a damped Lyα absorption (DLA) system at $z = 3.150$ observed in the spectrum of the quasar Q2233+131 at $z = 3.295$. The optical counterpart of this DLA has been identified and it shows a double-peaked Lyα emission line. Since one possible origin of DLAs at high redshift is an outflowing gas from star-forming galaxies, DLA 2233+131 provides a good laboratory to investigate the nature of high-z DLAs. Motivated by this, we have carried out ALMA band 8 observations to study the [C II] line in this system. However, we do not detect any significant emission line in the observed pass bands. Instead, we have serendipitously found three submm continuum sources in the observed sky area. One appears to be the quasar Q2233+131 itself while the other two sources are newly identified submm galaxies (SMGs), called SMG1 and SMG2 in this paper. They are located at a separation of 4.″7 and 8.″1 from Q2233+131, respectively. Their 646 μm fluxes are 6.35 mJy and 6.43 mJy, respectively, being higher than that of Q2233+131, 3.62 mJy. Since these two SMGs are not detected in the optical images obtained with the Hubble Space Telescope and the Subaru Telescope, they have a very red spectral energy distribution. It is, therefore, suggested that they

are high-redshift galaxies or very dusty galaxies at intermediate redshift, although we cannot rule out the possibility that they are optically very faint SMG analogs at low redshift. Follow-up observations will be necessary to explore the nature of this interesting region.

Key words: intergalactic medium — galaxies: high-redshift — quasars: absorption lines

1 Introduction

Quasar absorption line systems in ultraviolet (UV) spectra of high-redshift quasars have been used to investigate the nature of the intergalactic medium (IGM) and intervening objects such as gas-rich galaxies along lines of sight of quasars (Wolfe et al. 1986, 2005). Among such quasar absorption line systems, damped Lyα absorption (DLA) systems [N(H I) $\geq 2 \times 10^{20}$ cm^{-2} (Wolfe et al. 1986)] as well as Lyman limit systems (LLSs) [10^{17} cm$^{-2} \leq N$(H I) $< 2 \times 10^{20}$ cm^{-2} (Péroux et al. 2003)], and metal-line absorbers like Mg II absorbers (Bergeron & Boissé 1991; Steidel 1995b; Rao et al. 2006, 2011; Monier et al. 2009), are useful in studying the evolution of gas-rich galaxies from high through intermediate to low redshifts. However, one serious problem is that their optical counterparts are rarely identified (Wolfe et al. 2005; Krogager et al. 2017). Moreover, even when they are identified, their impact parameters are sometimes large, several tens of kpc to more than 100 kpc; e.g., Rao et al. (2011), Fynbo et al. (2018), and Mackenzie et al. (2019).

Christensen et al. (2014) examined the mass–luminosity (MZ) relation for DLAs (e.g., Møller et al. 2013) to find that the stellar masses of optical counterparts of DLAs show a good agreement with those predicted by the MZ relation, at least for the metal-rich DLAs. Krogager et al. (2017) showed that the low detection rate of optical DLA counterparts and the distribution of impact parameters between DLAs and background quasars are explained by a simple scenario where the "metallicity–luminosity relation" of a DLA is given by $M_{\rm UV} = -5 \times [{\rm M/H} + 0.3] - 20.8$ and the cross-section of the DLA is proportional to the luminosity following the relation $\sigma_{\rm DLA} \propto L^{0.8}$.

An open question for the nature of high-z DLAs is how the counterpart makes the absorption feature. The most probable candidates are disks of gas-rich galaxies including dwarf and low-surface brightness ones (e.g., Prochaska & Wolfe 1997, 1998; Jimenez et al. 1999). On the other hand, in the past two decades, the following new ideas have been proposed; galactic outflows (e.g., Taniguchi & Shioya 2000; Nagamine et al. 2004), tidal tails in the galaxy interaction (e.g., Kacprzak et al. 2010), and cosmic filaments (e.g., Fumagalli et al. 2017).

In the case of DLAs with a larger impact parameter, outflowing gas is a good candidate of the origin of absorption feature. For example, Taniguchi & Shioya (2000) proposed that an initial starburst in a galaxy with mass of $\sim 10^{11}\,M_\odot$ makes a large-scale shocked gaseous shell around the galaxy because of the superwind outflow. Since its typical radius reaches to ~ 100 kpc, this can explain the observed large impact parameters of DLAs. The galaxy itself could become fainter during the course of its passive evolution, making it difficult to identify optical counterparts in many cases, which would then explain the observed low detection rate of DLA counterparts in the optical. The metal enrichment by Type II supernovae gives a typical metallicity of $Z \sim 0.02\,Z_\odot$ or [M/H] ~ -1.7 in the shocked shell, consistent with the observed metallicity of DLAs. According to Taniguchi and Shioya (2001), the shock velocity ranges from $\sim$0 km s^{-1} to a few thousand km s^{-1}, depending on the energy of a superwind, the evolutional phase of a superwind, and the viewing angle towards a part of the shocked shell. They also found a positive correlation between the metallicity and velocity width, being consistent with the observed velocity–metallicity relation of high-z DLAs (e.g., Ledoux et al. 2006). Such superwind models can also explain the observed H I column density distribution function (Nagamine et al. 2004). Although it is unclear whether or not the galactic outflow is a major origin of high-z DLAs, some DLAs at high redshift with evidence for outflows have been observed so far (e.g., Christensen et al. 2004; Krogager et al. 2013; Kashikawa et al. 2014). To understandvthe nature of high-z DLAs, it is important to confirm the plausible origin of each DLA.

Optical observations even with the largest and most sensitive telescopes are extremely challenging because these systems are extremely faint in the optical due to cosmological surface brightness dimming, whereas millimeter/submillimeter windows offer a relatively constant flux due to the negative K-correction. Therefore, instead of the optical window, we are now able to choose the millimeter/submillimeter windows using the Atacama Large Millimeter and Submillimeter Array (ALMA). In fact, recently, ALMA has been used to investigate the nature of high-redshift DLA counterparts by using dust continuum emission and radio atomic and molecular emission lines such as [C II] 158 μm and CO emission lines (Neeleman et al. 2016, 2017, 2018, 2019; Fynbo et al. 2018; Kanekar

Table 1. Positional information of Q2233+131 and DLA 2233+131.

Q2233+131			
α(J2000.0)	δ(J2000.0)	z	Ref.*
22:36:19.19	+13:26:20.30	3.295	(1)
DLA 2233+131			
Relative offset from DLA 2233+131			
$\Delta\alpha$ ($''$)	$\Delta\delta$ ($''$)	z	Ref.*
+0.8	−2.1	3.150[†,‡]	(2)
+1.0	−2.1	3.151	(3)
+1.0	−2.3	3.1501	(4)
+0.9	−2.2	3.108–3.157[§]	(5)

*References: (1) SDSS DR5, (2) Djorgovski et al. (1996), (3) Steidel et al. (1995a); N1 in their table 12, (4) Møller et al. (2002); N-16-1D, (5) Kashikawa et al. (2014).

[†]The value of $z_{\rm DLA}$ is taken from Lu et al. (1993).

[‡] $z_{{\rm Ly}\alpha,{\rm em}} = 3.1530 \pm 0.0003$ in Djorgovski et al. (1996).

[§]Since the narrowband filter NB502 ($\lambda_{\rm c}$ 5025 Å and $\Delta\lambda$ = 60 Å) is used in Kashikawa et al. (2014), the redshift coverage is shown here.

et al. 2018; Møller et al. 2018). Encouraged by these pioneering ALMA observations of high-redshift DLAs, in this study we focus on a $z = 3.150$ DLA system in the line of sight of Q2233+131 whose redshift is $z = 3.295$ (Christensen et al. 2004). Because the Lyα emission from this optical counterpart shows a double-peaked profile, a possible origin of this DLA is thought to be outflowing gas. Since this DLA has been well studied by optical observations (Djorgovski et al. 1996; Christensen et al. 2004, 2007; Kashikawa et al. 2014), it provides a good laboratory to examine the scenario for the origin of the DLA, by combining optical and submm properties.

The structure of this paper is as follows. In section 2, we summarize general properties of our target, DLA 2233+131. Section 3 describes the observations and data reduction. The results of our ALMA observations are shown in section 4. In section 5, we discuss possible scenarios to explain the origin of DLA 2233+131 and serendipitously detected submm galaxies (SMGs). Finally, we present our concluding remark in section 6. Throughout this paper, we adopt a flat cosmology with $\Omega_{\rm m} = 0.3$, $\Omega_\Lambda = 0.7$, and $H_0 = 70\,{\rm km\,s^{-1}\,Mpc^{-1}}$.

2 Our target: DLA 2233+131

Our target is DLA 2233+131, found toward the quasar Q2233+131 at $z = 3.295$ (see table 1). This is the first intervening DLA whose optical counterpart was identified in both Lyα emission and stellar continuum by Djorgovski et al. (1996). The H I column density of DLA 2233+131 has been measured as follows; $\log N({\rm H\,I})\ ({\rm cm^{-2}}) = 20.00$ (Lu et al. 1993), 20.2 (Curran et al. 2002), and 19.95 [SDSS DR5; see Kashikawa et al. (2014)]. Since all these values are smaller than $\log N({\rm H\,I})\ ({\rm cm^{-2}}) = 20.3$ required to define the DLA, strictly speaking, this absorber is not a DLA but a sub-DLA or a Lyman limit system (LLS); see Péroux et al. (2003). However, following Djorgovski et al. (1996), we refer to this absorber as DLA 2233+131 in this paper. Its optical image, obtained with the Hubble Space Telescope (HST), is shown in the right-hand panel of figure 2.

This DLA is located $2\farcs3$ away from the quasar at PA = 159°. The projected separation from the line of sight to Q2333+133 is ∼18 kpc. A summary of the position of DLA 2233+131 measured in the literature is given in table 1. Note that the presence of this DLA feature was already found by Sargent et al. (1989) and by Lu et al. (1993) and the quasar Q2233+131 was found in the Canada–France–Hawaii Telescope Blue Grens Quasar Survey Plates by Crampton et al. (1985).

After the optical identification of DLA 2233+131 by Djorgovski et al. (1996), a number of follow-up studies have been made to-date. First, its metallicity is found as [Fe/H] = −1.4 (Lu et al. 1997). Møller and Christensen (2020) re-derived the metallicity to be [Si/H] = −0.97 ± 0.13. Since Fe tends to be depleted by dust (e.g., Wolfe et al. 2005; Rafelski et al. 2014), we use [Si/H] as the metallicity of DLA 2233+131 throughout this paper. The Lyα emission-line region is further investigated by Christensen et al. (2004) and Kashikawa et al. (2014). Christensen et al. (2004) performed integral field spectroscopic (IFS) observations of this DLA 2233+131 to find a spatially extended Lyα blob with a size of ∼23 kpc ×38 kpc. However, the extended morphology of Lyα emission was not confirmed by higher spectral resolution IFS observations (Christensen et al. 2007). Christensen et al. (2007) claimed that the IFS data obtained by Christensen et al. (2004) is likely affected by the systematic noise. Furthermore, Kashikawa et al. (2014) found not an extended but a compact Lyα emission-line region at DLA 2233+131. Their analysis shows that its effective radius is $1\farcs35$, corresponding to 10.24 kpc, and the Sersic index is $n = 1.80$. Christensen et al. (2014) estimated the stellar mass of the counterpart of DLA 2233+131 to be $\sim 10^{9.8}\,M_\odot$ based on their SED fitting. The observational properties of DLA 2233+131 are summarized in table 2. It is noted that another absorber at $z = 2.543$ is also identified in the UV spectrum of Q2233+131 (Steidel et al. 1995a). However, we call the absorber at $z = 3.150$ DLA 2233+133 in this paper.

3 Observations and data reduction

We observed a sky area with a radius of 11″ centered at the position of Q2233+131 in ALMA Cycle 5 (Proposal ID 2017.1.00345.S, PI: Y. Taniguchi). The observations

Table 2. Previously reported properties of the optical counterpart of DLA 2233+131.

Redshift ($z_{\rm DLA,em}$) of the counterpart measured from its emission line			
$z_{\rm DLA,em}$		References	Note
3.1476		Christensen et al. (2004)	
Impact parameter (b)			
b			
[$''$]	[kpc]	References	Note
2.3	17.5	Steidel et al. (1995a)	Broad-band imaging
2.3	17.5	Djorgovski et al. (1996)	Long-slit spectroscopy
2.37	18.0	Christensen et al. (2004)	IFS
2.41	18.3	Kashikawa et al. (2014)	Narrow-band imaging
Photometric measurements			
Measurements		References	Note
$V = 25.1$, $R = 24.8$		Steidel et al. (1995a)	
$H = 25.34$		Warren et al. (2001)	HST/NICMOS
$V_{50} = 25.75$		Møller et al. (2002)	V_{50} is a V-band filter of HST/STIS
$V > 24.40$, $R > 24.44$, $N502 = 24.30$		Kashikawa et al. (2014)	N502 is a narrow-band filter of Subaru/FOCAS ($\lambda_{\rm eff} = 5025$ Å, FWHM = 60 Å)
Lyα flux measurements			
Measurements		References	Note
$(6.4 \pm 1.2) \times 10^{-17}$ [erg s^{-1}]		Djorgovski et al. (1996)	Broad-band imaging
$(2.8 \pm 0.3) \times 10^{-16}$ [erg s^{-1}]		Christensen et al. (2004)	IFS, overestimated*
24.30 [AB mag]		Kashikawa et al. (2014)	Narrow-band imaging

*Christensen et al. (2007)

were conducted on 2018 May 24 using 46 12 m antennas with baseline lengths of 15.0–313.7 m. We used the ALMA Band-8 receivers to detect redshifted [C II] 158 μm and continuum emissions from the counterpart of DLA at $z = 3.150$ along the sightline to Q2233+131. We used four bands with a width of 1.875 GHz which are divided into 128 channels. We set the central frequency of the band to be 457.329 GHz and 459.121 GHz for the [C II] line, and 469.329 GHz and 471.121 GHz for the continuum emission. The total on-source integration time was 31.7 min.

All the data were reduced by using the Common Astronomy Software Application (CASA) ver 5.4.0 (McMullin et al. 2007). To search for the emission line, we create a dirty cube per 100 km s^{-1} bin. We then applied the uvcontsub task for each side band to make the final cube with the natural weighting. As for the continuum emission, we first created a dirty map with natural weighting using all four spectral windows. We then performed tCLEAN down to 2σ, resulting that we detected three continuum sources, one of which is Q2233+131. We detected no other objects with $>3\sigma$. Here, the 1σ noise level is $\sim$67 μJy beam^{-1} at the phase center. The synthesized beam size is $0\farcs84 \times 0\farcs61$ with a position angle of 52°. The maximum recoverable scale is $5\farcs15$. Flux measurements were performed via Gaussian fitting with the CASA task, imfit. We extracted spectra of these three continuum sources by adopting $1\farcs0$ diameter aperture.

4 Results

4.1 The ALMA Band 8 image

In figure 1, we show the obtained ALMA Band 8 image around the quasar Q2233+131. The field of view shown in figure 1 is approximately $22''$ in diameter. However, note that the sky area in which the primary beam response exceeds 50 percent is $13''$ in diameter (the inner dotted circle in figure 1), and that above 30 percent is $16\farcs5$ in diameter (the outer dashed circle in figure 1).

As shown in this figure, we have detected three bright continuum sources. One is the quasar Q2233+131 itself that is located in the center of the field of view. Since the observed optical rest-frame magnitudes of Q2233+131, $B = 18.29$ and $V = 18.15$ (Djorgovski et al. 1996) are brighter by $\sim$7 mag than those of DLA 2233+131 (see table 2), we assume that the most submm emission comes not from DLA 2233+131 but from Q2233+131. In figure 2, we compare ALMA band 8 and HST images around Q2233+131. We find no continuum source at the position of the optical counterpart of DLA 2233+131.

The other two continuum sources are unknown ones that are considered to be SMGs although their redshifts are also unknown. Hereafter, we call them SMG1 and SMG2 in this paper. Their angular distances from Q2233+131 are $4\farcs7$ and $8\farcs1$, respectively. In table 3, we give basic observational properties of the above three bright continuum sources. We

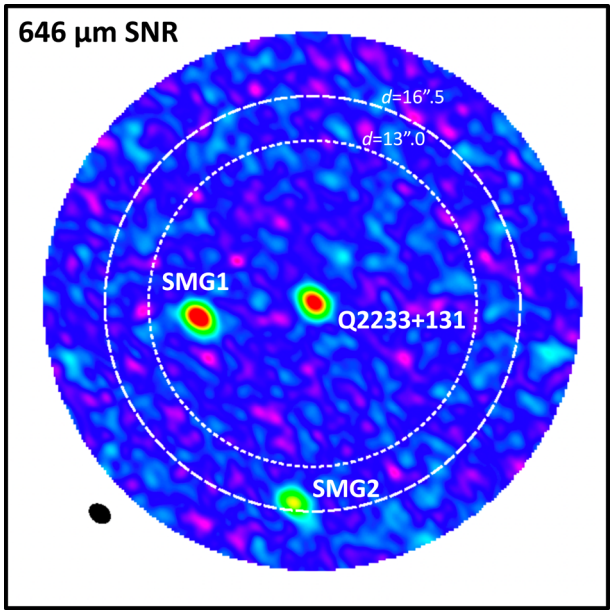

Fig. 1. ALMA rest-frame 646 μm continuum map (S/N) of the DLA 2233+131/Q2233+131 field (north is up and east is to the left). The field-of-view of the image is ∼22″ in diameter. The dotted inner and dashed outer circles indicate the area where the primary beam response exceeds 50% and 30%, respectively. The black field circle in the lower left-hand corner indicates the FWHM size of the PSF (0.″84 × 0.″61 with a position angle of 52°). (Color online)

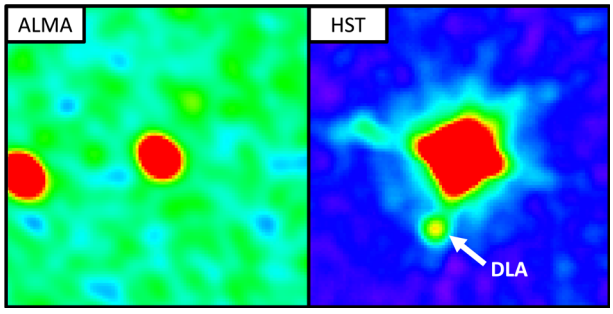

Fig. 2. Comparison of our ALMA image with the HST optical image around Q2233+131 (10″ × 10″). The ALMA rest-frame 646 μm continuum map (left) is compared with the HST WFPC2 F702W image (right) around DLA 2233+131/Q2233+131. The ALMA source shown at the left edge in the left-hand panel is SMG1 (see figure 1). (Color online)

here note that the newly found SMGs are brighter by a factor of two than the quasar Q2233+131.

4.2 The ALMA Band 8 spectra of DLA 2233+131, SMG1, and SMG2

In figure 3, we show the obtained spectrum of DLA 2233+131 together with those of Q2233+131, SMG1, and SMG2. None of these objects show significant emission lines at any observed frequency intervals. Here we use a 1″ aperture for all these sources. Since the frequency coverage of our band 8 observations is from 456.5 GHz to 459.8 GHz and from 468.5 GHz to 471.8 GHz, our non-detection means that [C II] 158 μm emission does not appear at the redshift intervals of $z = 3.028$–3.057 or $z = 3.133$–3.163.

Table 3. Flux measurements.

Objects	RA	Dec	$S_{646\mu m}$ [mJy]*
Q2233+131	22:36:19.19	+13:26:20.30	3.62† ±0.10
SMG 1	22:36:19.51	+13:26:19.71	6.35 ± 0.17
SMG 2	22:36:19.25	+13:26:12.29	6.43 ± 0.47

*This value is thought to come not from DLA 2233+131 but mostly from Q2233+131 (see text).
†Integrated flux density.

Now, let us estimate the upper limit of [C II] 158 μm emission line using a velocity-integrated map. Here, we use the following three methods. Method A: Aperture photometry at the Q2233+131 position with an aperture of 0.″5 in radius, Method B: Standard deviation of 300-point random aperture photometry with an aperture of 0.″5 in radius, and Method C: rms of the map in units of mJy beam^{-1}. To carry out these estimates, we first combine images with two velocity intervals, 200 km s^{-1} and 700 km s^{-1}. These two intervals correspond to a typical FWHM for a star-forming galaxy and the lowest FWHM of Lyα emission observed by Christensen et al. (2004). The velocity center is set to be 458.184 GHz at which [C II] 158 μm emission is expected to be detected at $z_{\rm DLA}$. The results are summarized in table 4. Although we do not know which is the best estimate, here we adopt the result of Method B with FWHM([C II]) = 700 km s^{-1}. In this case, the 3σ velocity weighted upper limit is estimated as 330 mJy km s^{-1}.

5 Discussion

5.1 Why no detection in [C II] from DLA 2233+131?

As described in section 4, we cannot detect [C II] 158 μm emission from DLA 2233+131. However, the previous ALMA observations detected this emission from a sample of high-z DLAs at $z > 3.6$ except one target at $z = 4.6$ (Neeleman et al. 2017, 2019); see table 5. Although their impact parameters range from ∼20 kpc to ∼40 kpc, the velocity coverage of [C II] 158 μm emission is nearly the same as that of DLA, the detected [C II] 158 μm emission appears to come from the object associated with the DLA in each case. The observed large impact parameters from a few to several tens of kpc are significantly larger than typical sizes of such high-z galaxies. It is thus suggested that

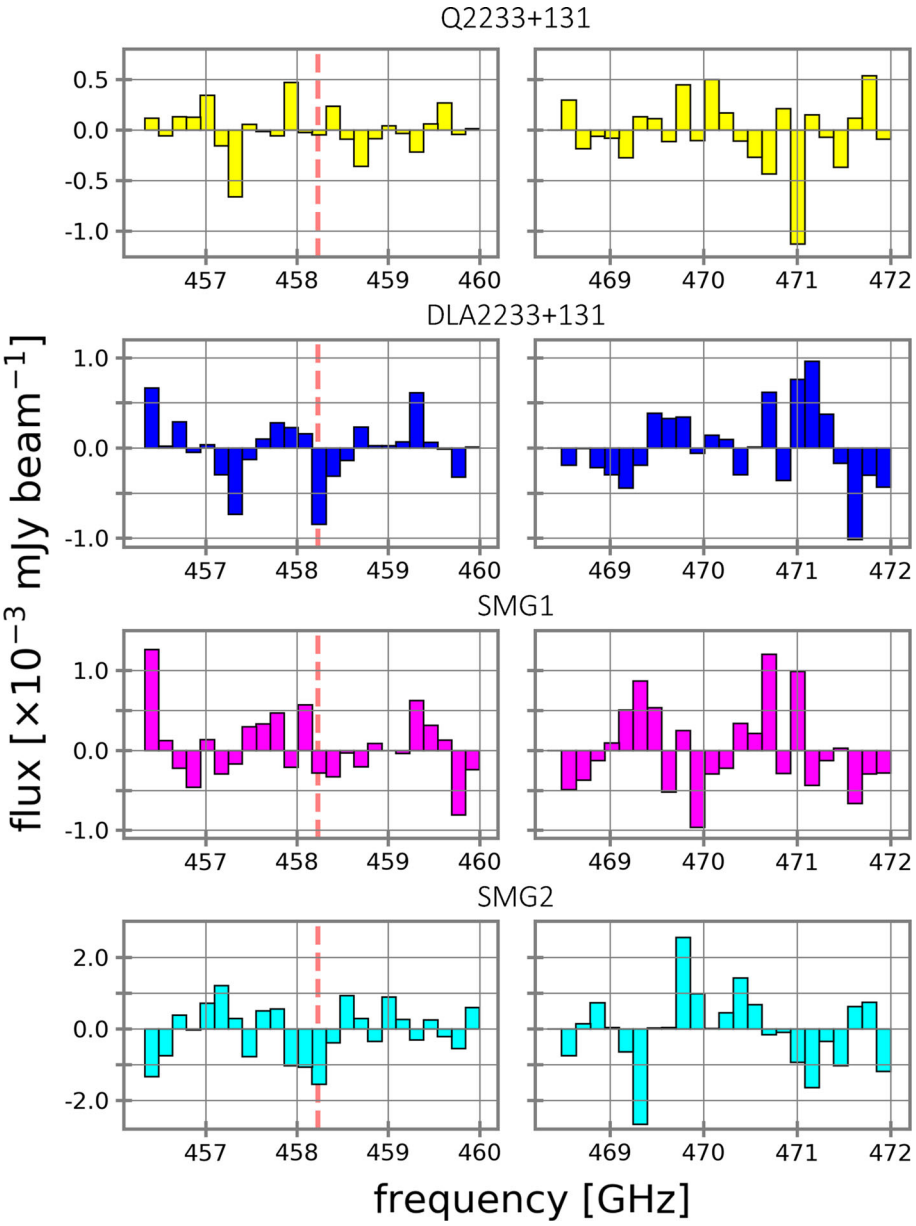

Fig. 3. Spectra of Q2233+131, DLA 2233+131, SMG1, and SMG2. Our ALMA band 8 spectra of Q2233+131, DLA 2233+131, SMG1, and SMG2. The red dashed line in each panel indicates expected observed-frame frequency of the [C II] line at $z = 3.150$. (Color online)

Table 4. Various estimates of the 1σ upper limit of [C II] 158 μm emission for DLA 2233+131.

FWHM([C II])	Method A (mJy km s^{-1})	Method B (mJy km s^{-1})	Method C (mJy beam^{-1})
200 km s^{-1}	75	61	91
700 km s^{-1}	24	110	160

these DLA counterparts have a large halo of dense, neutral gas around them.

Possible origins of such large halos are considered to be either outflows from a DLA counterpart or cooling flows from primordial gas in cosmic webs. Our target DLA 2233+131 has an evident optical counterpart observed in both the Lyα emission line and the UV continuum. The presence of the double-peaked Lyα emission line (Christensen et al. 2004) is considered as evidence for outflowing gas. However, no [C II] 158 μm emission is detected in our observations. Therefore, it is important to consider possible reasons for this non-detection.

A simple explanation is that our observations are too shallow to detect the [C II] 158 μm emission line. Indeed, previously detected [C II] lines from high-z DLAs are fainter than our detection limit (see table 5). We estimate a probable expected flux of [C II] 158 μm emission using the Lyα emission line flux obtained by Djorgovski

Table 5. Summary of [C II] observations of DLA with ALMA.

z_{DLA}	Quasar	$\log N_{HI}$	[M/H]	b		f(line)	FWHM	SFR	Ref.*
				[″]	[kpc]	[mJy km s^{-1}]	[km s^{-1}]	[$M_\odot$ yr^{-1}]	
4.2584	J0817+1351	21.30 ± 0.15	-1.15 ± 0.15 (S)†	6.2	42	13.1	460 ± 50	110 ± 10	(1)
3.5795	J1201+2117	21.35 ± 0.15	-0.747 ± 0.15 (Si)†	2.5	18	7.1	330 ± 50	24 ± 8	(1)
4.3900	J0834+2140	21.30 ± 0.10	-1.30 ± 0.20 (S)†	4.0	27	173	270 ± 60§	7 ± 2	(2)
4.3446	J1101+0531	21.00 ± 0.20	-1.07 ± 0.12 (Si)†	4.0	27	62	370 ± 60§	<7	(2)
4.6001	J1253+1046	20.30 ± 0.15	-1.36 ± 0.16‡	—	—	<42	—	<9	(2)
4.2241	PSS1443+2724	21.10 ± 0.10	-0.95 ± 0.20‡	2.3	16	846	510 ± 60§	15 ± 4	(2)
3.150	Q2233+131	19.95–20.20	-0.97 ± 0.13 (Si)	2.3	18	< 330	—	22 ± 12	(3)

*References: (1) Neeleman et al. (2017), (2) Neeleman et al. (2019), (3) This work.
†Measured by Rafelski et al. (2012).
‡[M/H] = [Fe/M] + 0.3 dex (Rafelski et al. 2012).
§These values correspond to ΔV_{90}, the velocity width encompassing 90% of the integrated optical depth,(e.g., Prochaska & Wolfe 1997).

et al. (1996); $f(\mathrm{Ly}\alpha) = (6.4 \pm 1.2) \times 10^{-17}$ erg cm^{-2} s^{-1}. Using the luminosity distance to DLA 2233+131, $D_L = 26951.9$ Mpc given the cosmological parameters adopted in this paper, we obtain the Lyα luminosity, $L(\mathrm{Ly}\alpha) = 5.5 \times 10^{42}$ erg s^{-1}. Adopting the case B recombination case, the Lyα/Hα intensity ratio of 8.7, we obtain the Hα luminosity, $L(\mathrm{H}\alpha) = 6.4 \times 10^{41}$ erg s^{-1}. Based on this Hα luminosity, we can estimate the star formation rate, SFR $\sim 5 M_\odot$ yr^{-1}. Then, we use the relation of SFR($M_\odot$yr^{-1}) = $7.9 \times 10^{-42} L(\mathrm{H}\alpha)$ [erg s^{-1}] (Kennicutt 1998). Using this SFR, we estimate the far-infrared (FIR) luminosity: L(FIR) = 1.1×10^{44} erg s^{-1}, where FIR means the wavelength interval between 1 μm and 1000 μm. Here, we use the relation SFR($M_\odot$ yr^{-1}) = $4.5 \times 10^{-44} L$(FIR) [erg s^{-1}] (Kennicutt 1998). Adopting the [C II] 158 μm emission to FIR luminosity ratio of $10^{-2.5}$ for L(FIR) < $10^{12} L_\odot$ (Luhman et al. 2003; Maiolino et al. 2009), we obtain the expected [C II] 158 μm emission luminosity, $L([\mathrm{C\,II}]) = 3.7 \times 10^{41}$ erg s^{-1}. Now, we can estimate the expected velocity-integrated flux of [C II] 158 μm emission as $S([\mathrm{C\,II}])\,\delta v = L([\mathrm{C\,II}])\,(1+z)(1.04 \times 10^{-3})^{-1} \nu_{\mathrm{rest}}([\mathrm{C\,II}])\,D_L^{-2}$, where $z = 3.150$, $\nu_{\mathrm{rest}}([\mathrm{C\,II}]) = 1900.5$ GHz, and $D_L = 26951.9$ Mpc (Solomon & Vanden Bout 2005). We then obtain $S([\mathrm{C\,II}])\,\delta v = 302$ mJy km s^{-1}. This is lower than the 3σ limit of our observations (330 mJy km s^{-1}), as discussed in subsection 4.2.

Here, it should be noted that the [C II]/FIR relation of high-z galaxies shows a broad scatter (Carilli & Walter 2013; Malhotra et al. 2017) ranging from [C II]/FIR $\sim 10^{-3.6}$–$10^{-1.5}$. Based on this, the estimated [C II] flux range is $S([\mathrm{C\,II}])\,\delta v = 24$–$3200$ mJy km s^{-1}. The non-detection of [C II] emission from DLA 2233+131 implies the low [C II]/FIR ratio of DLA 2233+131. Malhotra et al. (2017) showed that the main determining factor for the [C II]/FIR ratio is the dust temperature; lower values of [C II]/FIR suggest higher dust temperatures. On the other hand, we have not detected the dust continuum emission from DLA 2233+131. Moreover, Christensen et al. (2004) estimate the SFR of DLA 2233+131 not only from the Lyα luminosity but also from the broad-band photometry, SFR(UV) = $12 \pm 5\ M_\odot$ yr^{-1}. The SFR(Lyα)/SFR(UV) ratio of DLA 2233+131 is comparable to those of high-z Lyα emitters, suggesting that the DLA 2233+131 host galaxy has only little dust content. Therefore, there could be other possibilities for the reason why [C II] emission has not been detected.

A possible explanation is that the DLA counterpart is optically thick enough to activate the self-shielding effect (Worseck et al. 2014). In this scenario, the [C II] emission line is expected to be unobservable because the photodissociation region (PDR) cannot be formed. This is consistent with almost all hydrogens in systems with $N_{\mathrm{H\,I}} > 10^{19.5}$ being likely neutral (Viegas 1995). Although Christensen et al. (2007) and Kashikawa et al. (2014) did not confirm the greatly extended structure of DLA 2233+131 reported by Christensen et al. (2004), there appear to be some faint Lyα-emitting regions to the east of the galaxy associated with an idea that the DLA (see figure 2 of Christensen et al. 2007 and figure 2 of Kashikawa et al. 2014). Christensen et al. (2004) reported that the Lyα emission line from DLA 2233+131 shows a double peak profile which is confirmed by the follow-up observations with a higher spectral resolution performed by Christensen et al. (2007). These properties suggest the existence of the outflowing gas. If an optically thick scenario is the case, the origin of the faint Lyα emission in the eastern part of the counterpart of DLA 2233+131 can be explained by the resonant scattering. This scenario is similar to that proposed by Christensen et al. (2004), where Lyα photons radiated by star-forming regions are scattered by surrounding H I clouds that are extended by the galactic outflow, although its spatial extent is not so large.

In summary, we have estimated the [C II] 158 μm flux to be $S([\mathrm{C\,II}])\ \delta v = 24$–$3200$ mJy km s^{-1} based on the SFR of the counterpart. A large spread of the estimated flux is due to a broad scatter of observed [C II]/FIR ratio. Our non-detection suggests a low [C II]/FIR value, and the exposure time of our observations may be too short to detect [C II] emission from DLA 2233+131. Indeed, most of the previously detected [C II] emission from high-z DLAs is fainter than the limiting flux of our observations (Neeleman et al. 2017, 2019). Thus it is recommended that a new observation with a longer integration time should be executed in future. Although there is no guideline for integration time, a couple of hours' integration may be fine as a trial. Note that the previous successful detection of [C II] 158 μm emission from DLAs at $z \sim 4$ was made with an integration time of a couple of hours (Neeleman et al. 2017, 2019).

5.2 What are the two SMGs ?

We have serendipitously found two SMGs in the Q2233+131 field, SMG1 and SMG2 (see figure 1 and table 3). In this subsection, we discuss their origins.

5.2.1 Basic properties of SMGs

The projected separations from SMG 1 and 2 to Q2233+131 are 4.″7 and 8.″1, respectively. At present, we have no direct information on their redshifts. We search for the data available to-date to estimate their redshifts.

First, in order to search for their optical counterparts, we examine the HST Wide Field and Planetary Camera (WFPC) F702W and HST Near Infrared Camera and Multi Objects Spectrometer (NICMOS) F160W images of the Q2233+131 field in the upper central and upper right-hand panel of figure 4, respectively. However, we find no optical counterpart. Note that these images were retrieved from the HST archive by Christensen et al. (2004) (see their figure 7) and Warren et al. (2001) (N16 in their figure 8), respectively. As for a HST/STIS high-resolution image for DLA 2233+131, see Møller et al. (2002), in which DLA 2233+131 is called as N-16-1D. However, since only a 4″ by 4″ area is displayed, the two SMGs are not found there. Next, Kashikawa et al. (2014) obtained broad- and narrow-band images of the Q2233+131 field to find an optical counterpart of DLA 2233+131 using the Faint Object Camera and Spectrograph (FOCAS; Kashikawa et al. 2002) on the Subaru Telescope. We again find no optical counterpart at the position of the SMGs in their FOCAS images (see the lower two panels of figure 4). The 3σ limiting AB magnitudes of FOCAS images in a 2″ aperture are $B = 24.40$ and $V = 24.44$, respectively.

We then checked MIR and FIR images obtained by Wide-field Infrared Survey Explorer (WISE; Wright et al. 2010) in the framework of the ALLWISE program (Cutri et al. 2014). Although the Q2233+131 itself is detected in all the WISE band images (3.4, 4.6, 12, and 22 μm), the spatial resolution of WISE (6.″1–12.″0, depending on bands) is not high enough to resolve the quasar and the two SMGs. Note that no image around the Q2233+131 field had been taken by the Spitzer Space Telescope.

It has been reported that most samples of previously observed SMGs are high-z objects with a median redshift of $z \sim 2.5$ and that $\sim$20% of SMGs are at $z > 3$ (e.g., Chapman et al. 2005; Yun et al. 2012; Danielson et al. 2017). At low redshifts, Oteo et al. (2017) defined the $z < 0.5$ analogs of SMGs based on their dust temperatures and total IR luminosities. All of these low-z SMG analogs are detected in optical observations. However, since low-z SMG analogs are selected by utilizing available spectral redshift, the samples may be biased toward optically bright ones. Yun et al. (2012) found some SMGs at $z < 1$ in their deep submm imaging survey. All the SMGs at $z < 1$ confirmed by them are brighter than $i = 23.5$ mag. Danielson et al. (2017) confirmed spectroscopic redshifts of 73 SMGs with the Keck Telescope. 12 out of the 73 SMGs are at $z < 1$ and all of them are brighter than $R = 24.2$. As for $1 < z < 1.5$ SMGs, 75% (6/8) of them have $R < 23.8$. Again, we note that these samples may be biased toward optically bright objects. Taking account of the non-detection of SMG1 and SMG2 in the optical with HST and the Subaru Telescope, it is more likely that these SMGs are located at high redshifts. While we found that the two SMGs are dusty and invisible at shorter wavelengths, it is hard to derive photometric redshifts for them due to the limited photometric points available at present.

5.2.2 Are the two SMGs associated with Q2233+131 at $z = 3.3$?

Since we cannot derive any secure redshifts of the SMGs by utilizing the current dataset, we discuss their possible association to Q2233+131 based on our ALMA data. Because both of these SMGs show no [C II] emission line as shown in figure 3, they may not be associated to DLA 2233+131 at $z = 3.150$. Hence, we discuss their association to Q2233+131.

SMG1 and SMG2 are located in the sky area within a diameter of 16.″5, in which the primary beam response exceeds 30 percent. In this case, the presence of the three sources, SMG1, SMG2, and Q2233+131, gives a surface number density of 1.4×10^{-2} arcsec^{-2}, corresponding to $\sim$50.4 deg^{-2}. We compare this surface density with that obtained by the ALMA 26 arcmin^2 survey of GOODS-S at one millimeter (ASAGAO) survey (Hatsukade et al. 2018). According to the ASAGAO survey, the surface number density of SMGs at $z \sim 3$ is estimated as $\sim$900 deg^{-2} for

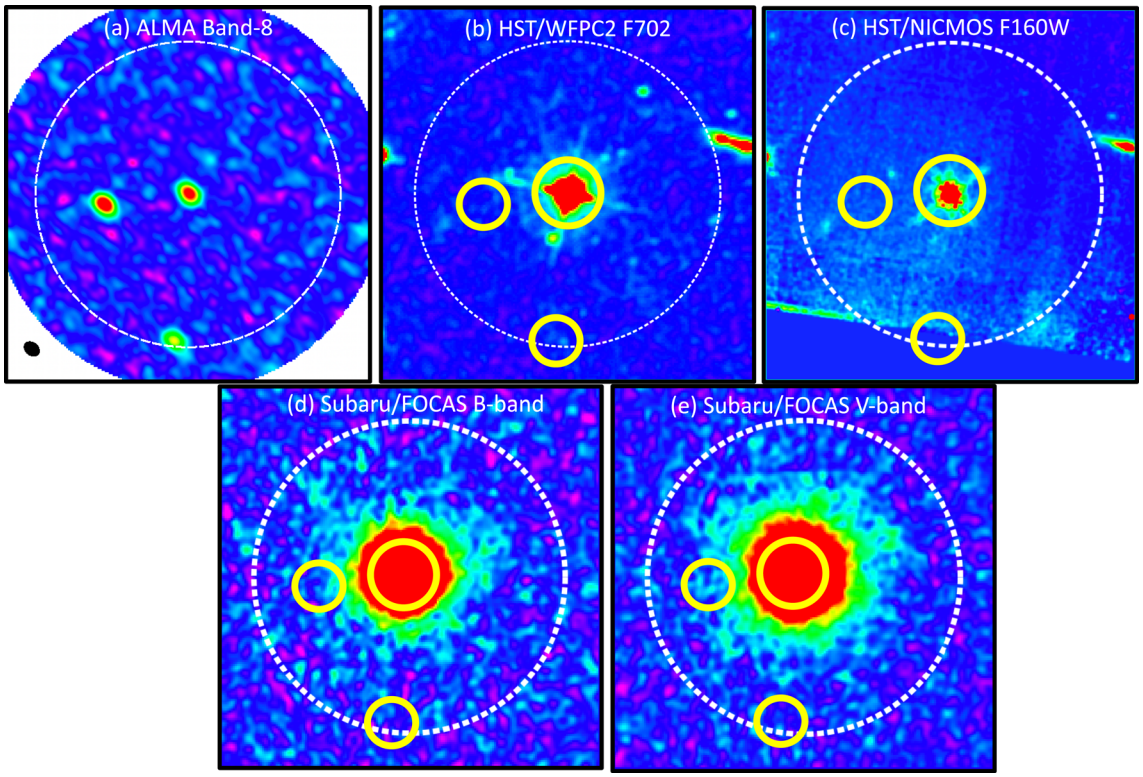

Fig. 4. Comparison between ALMA band 8 image (upper left) and optical images of the Q2233+131 field (20″ × 20″); (a) ALMA 646 μm, (b) HST WFPC2 F702W, (c) HST NICMOS F160W, (d) Subaru FOCAS B, and (e) Subaru FOCAS V image. Three continuum sources, Q2233+131, SMG1, and SMG2, are shown by yellow circles. The dashed circle in the panels (b), (c), (d), and (e), shows a sky area with a diameter of 16.″5. (Color online)

SMGs with their flux density of $S > 1$ mJy at $\lambda = 1.2$ mm, giving a surface number density of 4.7×10^{-4} arcsec^{-2}. Here we estimate the flux densities at $\lambda = 1.2$ mm of the two SMGs, SMG1 and SMG2, and the quasar Q2233+131. If we adopt a typical SED for SMGs at ∼3 (Swinbank et al. 2014), we obtain 1.4 mJy, 1.4 mJy, and 1.0 mJy for the three sources. Therefore the surface density of SMGs with their flux density of $S > 1$ mJy at $\lambda = 1.2$ mm is kept as 1.4×10^{2} arcsec^{-2}. It is here noted that the quasar Q2233+131 is also included as an SMG. This surface number density is higher by a factor of ∼30 than that obtained with the ASAGAO project. Note that, when we do not limit to $z \sim 3$, the cumulative surface number density of ASAGAO SMGs with flux density of $S_{\lambda} > 1.350$ mJy (the brightest bin) at $\lambda = 1.2$ mm is $4.2^{+4.1}_{-2.3} \times 10^{2}$ deg^{-2} (see table 4 of Hatsukade et al. 2018 for further details). This is ∼8 times higher than the SMG surface number density of our target field.

The obtained high surface number density with respect to that of the ASAGAO survey suggests that the two SMGs and Q2233+131 are located in an over-density region at $z \sim 3$. This also suggests that our target region comprises a so-called quasar–SMG association (e.g., Fu et al. 2017; Trakhtenbrot et al. 2017). Their typical separations are ∼10–100 kpc. Such quasar-SMG systems are considered to be gas-rich merging systems (e.g., Guilloteau et al. 1999; Wang et al. 2013; Willott et al. 2013; Fu et al. 2017). If SMG1 and SMG2 are located at the same redshift as that of Q2233+131, $z = 3.3$, their projected distances from Q2233+131 are 35.2 kpc and 60.2 kpc, respectively. If this is the case, the environment around Q2233+131 provides a good laboratory for future investigations of a merging system at such a high redshift. We note that most of previously discovered gas-rich merging systems are identified as an unresolved single SMG by using either Herschel or WISE, whereas they contain multiple submm sources based on ALMA observations. Here we note again that our three systems (one quasar with the two SMGs) are also a single source in the WISE observation.

However, currently, there are no lines of secure evidence for their physical association. Future follow-up observations will be important to examine this scenario. If the SMG is an optically faint object at low redshift, we may be able to measure its redshift by deep optical spectroscopic observations such as very sensitive long-slit or integral field spectroscopy. If the SMGs are too faint to detect even with very deep optical spectroscopy, ALMA is the best telescope for the redshift measurement. The next step will be a search for [C II] 158 μm emission at the Q2233+131 redshift, $z \sim 3.3$. If there is still no detection, another plan is to carry out

spectral scan observations. In this case, CO emission lines may be useful because such SMGs have been forming stars with a high SFR and thus it is expected that there is a lot of molecular gas in them. In this case, CO(3–2) or CO(4–3) seems a better choice, if $z \sim 2$–3, because this line can be detected at Band 3, the observing condition of which is generally better than that at Band 8 in the ALMA site; e.g., Fynbo et al. (2018) and Neeleman et al. (2018). If the SMGs are at $z < 1$, the CO(2–1) line is useful for the redshift measurement (e.g., Møller et al. 2018).

6 Summary

We have conducted ALMA Band-8 observations of DLA 2233+131 at $z = 3.150$ found in the UV spectrum of quasar Q2233+131 at $z = 3.295$. This DLA is the first intervening DLA at high redshift whose optical counterpart was identified (Djorgovski et al. 1996). The Lyα emission associated with this DLA shows double peak profile whose separation corresponds to 600–750 km s^{-1}(Christensen et al. 2004). High spectral resolution IFS observations by Christensen et al. (2007) and an excellent quality image obtained by Kashikawa et al. (2014) showed the optical counterpart of DLA 2233+131 is a compact galaxy, although some faint extended Lyα emitting regions appear to be associated.

To investigate the origin of this DLA, we have conducted ALMA Band 8 observations to detect [C II] 158 μm emission. However, we have not detected significant [C II] emission in our ALMA observations. A possible reason of this non-detection is that the line is too faint to be detected in the relatively short integration carried out here. We estimate the expected [C II] from DLA 2233+131 based on its SFR derived by optical observations, $S([\mathrm{C\,II}])\,\delta v = 24$–3200 mJy km s^{-1}. The large spread of estimated flux comes from the scatter of observed [C II]/FIR ratio. In the case that the [C II]/FIR ratio is significantly low, the expected [C II] flux is fainter than the detection limit of our ALMA observations. Although such a low [C II]/FIR value suggests a higher dust temperature (Malhotra et al. 2017), optical observations imply that DLA 2233+131 may have only little dust content. This is consistent with the non-detection of dust continuum from DLA 2233+131 in this work. Therefore, we consider another possible scenario in which the counterpart of DLA 2233+131 is optically thick enough to activate the self-shielding effect. In this scenario, the PDR cannot be formed and thus [C II] emission is not radiated. The observed double peak Lyα emission implies the existence of the outflowing gas. The origin of faint emissions around DLA 2233+131 may be explained by the resonant scattering.

The previous ALMA [C II] 158 μm or CO observations of from low- to intermediate- to high-z DLAs are successful (Neeleman et al. 2016, 2017; Fynbo et al. 2018; Kanekar et al. 2018; Møller et al. 2018; Neeleman et al. 2018, 2019). Although we cannot detect [C II] 158 μm emission from DLA 2233+131, we would like to recommend that one carry out a systematic search for [C II] 158 μm emission for a large sample of DLA from low to high redshifts. One problem is that it is difficult to estimate reasonable integration time because we do not have any reliable line flux estimators. Therefore, the first step is to carry out this survey with one hour integration for any DLAs. Such a large survey will tell us useful information on the origin of DLAs although there may be a variety of DLA counterparts, e.g., outflowing gas, or disks of gas-rich galaxies from dwarf to giant ones.

Despite the non-detection of [C II] 158 μm emission from DLA 2233+131, we have serendipitously found the two SMGs in the observed field; SMG1 and SMG2. Their angular separations from Q2233+131 are 4.″7 and 8.″1, respectively. They are not detected in the optical imaging with HST or the Subaru Telescope. Since most of previously observed low-z SMGs are also detected in optical observations, they may not be low-z galaxies although we cannot rule out the possibility that they are optically very faint low-z objects.

Because it is hard to drive the redshifts of SMG1 and SMG2, we consider the possibility that these two SMGs and Q2233+131 are associated with each other; i.e., SMG1 and SMG2 are at $z = 3.3$ as well as Q2233+131. If this is the case, the linear projected separations from the quasar to SMG1 and SMG2 are 35 and 60 kpc, respectively. These separations are similar to that of gas-rich merging systems observed as quasar-SMG pairs at high redshift (10–100 kpc). If this is the case, the Q2233+131 provides an interesting target to study gas-rich merging systems at high redshift. Because we cannot confine the redshifts of two SMGs, new ALMA and/or deep optical observations will be necessary to obtain their redshifts.

Acknowledgment

We are very grateful to the referee, Dr. Lise Chiristensen, for careful reading and many helpful comments. This paper uses the ALMA data ADS/JAO.ALMA#2017.1.00345.S. KO is grateful to Masahiro Nagasima for kindly giving many useful comments. This work is supported from Grants-in-Aid for Scientific Research (KAKENHI) provided by Japan Society for the Promotion of Science (JSPS) No. 16H02166 (PI: Y. Taniguchi). YT would like to thank Jason X. Prochaska for his kind communication for these years. Actually, he showed me ALMA observations made by his group prior to publication. We would also like to thank Kotaro Kohno for useful discussion

on the metallicity effect for the detection of [C II] 158 μm emission from DLAs.

References

Bergeron, J., & Boissé, P. 1991, A&A, 243, 344
Carilli, C. L., & Walter, F. 2013, ARA&A, 51, 105
Chapman, S. C., Blain, A. W., Smail, I., & Ivison, R. J. 2005, ApJ, 622, 772
Christensen, L., Møller, P., Fynbo, J. P. U., & Zafar, T. 2014, MNRAS, 445, 225
Christensen, L., Sánchez, S. F., Jahnke, K., Becker, T., Wisotzki, L., Kelz, A., Popović, L. Č., & Roth, M. M. 2004, A&A, 417, 487
Christensen, L., Wisotzki, L., Roth, M. M., Sánchez, S. F., Kelz, A., & Jahnke, K. 2007, A&A, 468, 587
Crampton, D., Schade, D., & Cowley, A. P. 1985, AJ, 90, 987
Curran, S. J., Webb, J. K., Murphy, M. T., Bandiera, R., Corbelli, E., & Flambaum, V. V. 2002, PASA, 19, 455
Cutri, R. M., et al. 2014, VizieR Online Data Catalog, II/328
Danielson, A. L. R., et al. 2017, ApJ, 840, 78
Djorgovski, S. G., Pahre, M. A., Bechtold, J., & Elston, R. 1996, Nature, 382, 234
Fu, H., Isbell, J., Casey, C. M., Cooray, A., Prochaska, J. X., Scoville, N., & Stockton, A. 2017, ApJ, 844, 123
Fumagalli, M., et al. 2017, MNRAS, 471, 3686
Fynbo, J. P. U., et al. 2018, MNRAS, 479, 2126
Guilloteau, S., Omont, A., Cox, P., McMahon, R. G., & Petitjean, P. 1999, A&A, 349, 363
Hatsukade, B., et al. 2018, PASJ, 70, 105
Jimenez, R., Bowen, D. V., & Matteucci, F. 1999, ApJ, 514, L83
Kacprzak, G. G., Murphy, M. T., & Churchill, C. W. 2010, MNRAS, 406, 445
Kanekar, N., et al. 2018, ApJ, 856, L23
Kashikawa, N., et al. 2002, PASJ, 54, 819
Kashikawa, N., Misawa, T., Minowa, Y., Okoshi, K., Hattori, T., Toshikawa, J., Ishikawa, S., & Onoue, M. 2014, ApJ, 780, 116
Kennicutt, R. C., Jr. 1998, ARA&A, 36, 189
Krogager, J.-K., et al. 2013, MNRAS, 433, 3091
Krogager, J.-K., Møller, P., Fynbo, J. P. U., & Noterdaeme, P. 2017, MNRAS, 469, 2959
Ledoux, C., Petitjean, P., Fynbo, J. P. U., Møller, P., & Srianand, R. 2006, A&A, 457, 71
Lu, L., Wolfe, A. M., Turnshek, D. A., & Lanzetta, K. M. 1993, ApJS, 84, 1
Lu, L., Sargent, W. L. W., & Barlow, T. A. 1997, ApJ, 484, 131
Luhman, M. L., Satyapal, S., Fischer, J., Wolfire, M. G., Sturm, E., Dudley, C. C., Lutz, D., & Genzel, R. 2003, ApJ, 594, 758
Mackenzie, R., et al. 2019, MNRAS, 487, 5070
McMullin, J. P., Waters, B., Schiebel, D., Young, W., & Golap, K. 2007, in ASP Conf. Ser., 376, Astronomical Data Analysis Software and Systems XVI, ed. et al. (San Francisco: ASP), 127
Maiolino, R., Caselli, P., Nagao, T., Walmsley, M., De Breuck, C., & Meneghetti, M. 2009, A&A, 500, L1
Malhotra, S., et al. 2017, ApJ, 835, 110
Møller, P., et al. 2018, MNRAS, 474, 4039
Møller, P., & Christensen, L. 2020, MNRAS, 492, 4805
Møller, P., Fynbo, J. P. U., Ledoux, C., & Nilsson, K. K. 2013, MNRAS, 430, 2680
Møller, P., Warren, S. J., Fall, S. M., Fynbo, J. U., & Jakobsen, P. 2002, ApJ, 574, 51
Monier, E. M., Turnshek, D. A., Rao, S. M., & Weyant, A. 2009, AJ, 138, 1609
Nagamine, K., Springel, V., & Hernquist, L. 2004, MNRAS, 348, 435
Neeleman, M., et al. 2016, ApJ, 820, L39
Neeleman, M., Kanekar, N., Prochaska, J. X., Rafelski, M., Carilli, C. L., & Wolfe, A. M. 2017, Science, 355, 1285
Neeleman, M., Kanekar, N., Prochaska, J. X., Christensen, L., Dessauges-Zavadsky, M., Fynbo, J. P. U., Møller, P., & Zwaan, M. A. 2018, ApJ, 856, L12
Neeleman, M., Kanekar, N., Prochaska, J. X., Rafelski, M. A., & Carilli, C. L. 2019, ApJ, 870, L19
Oteo, I., et al. 2017, arXiv:1707.05329
Prochaska, J. X., & Wolfe, A. M. 1997, ApJ, 487, 73
Prochaska, J. X., & Wolfe, A. M. 1998, ApJ, 507, 113
Péroux, C., McMahon, R. G., Storrie-Lombardi, L. J., & Irwin, M. J. 2003, MNRAS, 346, 1103
Rafelski, M., Wolfe, A. M., Prochaska, J. X., Neeleman, M., & Mendez, A. J. 2012, ApJ, 755, 89
Rafelski, M., Neeleman, M., Fumagalli, M., Wolfe, A. M., & Prochaska, J. X. 2014, ApJ, 782, L29
Rao, S. M., Belfort-Mihalyi, M., Turnshek, D. A., Monier, E. M., Nestor, D. B., & Quider, A. 2011, MNRAS, 416, 1215
Rao, S. M., Turnshek, D. A., & Nestor, D. B. 2006, ApJ, 636, 610
Sargent, W. L. W., Steidel, C. C., & Boksenberg, A. 1989, ApJS, 69, 703
Solomon, P. M., & Vanden Bout, P. A. 2005, ARA&A, 43, 677
Steidel, C. C. 1995b, QSO Absorption Lines, ed. G. Meylan (Berlin: Springer-Verlag), 139
Steidel, C. C., Pettini, M., & Hamilton, D. 1995a, AJ, 110, 2519
Swinbank, A. M., et al. 2014, MNRAS, 438, 1267
Taniguchi, Y., & Shioya, Y. 2000, ApJ, 532, L13
Taniguchi, Y., & Shioya, Y. 2001, ApJ, 547, 146
Trakhtenbrot, B., Lira, P., Netzer, H., Cicone, C., Maiolino, R., & Shemmer, O. 2017, ApJ, 836, 8
Viegas, S. M. 1995, MNRAS, 276, 268
Wang, R., et al. 2013, ApJ, 773, 44
Warren, S. J., Møller, P., Fall, S. M., & Jakobsen, P. 2001, MNRAS, 326, 759
Willott, C. J., Omont, A., & Bergeron, J. 2013, ApJ, 770, 13
Wolfe, A. M., Turnshek, D. A., Smith, H. E., & Cohen, R. D. 1986, ApJS, 61, 249
Wolfe, A. M., Gawiser, E., & Prochaska, J. X. 2005, ARA&A, 43, 861
Worseck, G., et al. 2014, MNRAS, 445, 1745
Wright, E. L., et al. 2010, AJ, 140, 1868
Yun, M. S., et al. 2012, MNRAS, 420, 957